ARCHIVES OF MECHANICS
Arch. Mech. **74** (1), 3–12, 2022, DOI: 10.24423/aom.3871

Molecular dynamics study of the fracture of single layer buckled silicon monosulfide and germanium selenide

M.-Q. LE

Division of Mechanics of Materials and Structures, School of Mechanical Engineering, Hanoi University of Science and Technology, No. 1, Dai Co Viet Road, Hanoi, Viet Nam, e-mail: quy.leminh@hust.edu.vn

Molecular dynamics simulations were conducted with the Stillinger–Weber potential at room temperature to study the mechanical properties and find the mode-I critical stress intensity factor of buckled two-dimensional (2D) hexagonal silicon mono-sulfide (SiS) and germanium selenide (GeSe) sheets. Uniaxial tensile tests were simulated for pristine and pre-cracked sheets. 2D Young's modulus of SiS and GeSe are estimated at 38.3 and 26.0 N/m, respectively. Their 2D fracture strength is about 3.1–3.5 N/m. By using the initial crack length with the corresponding fracture stress, their mode-I critical stress intensity factor is estimated in the range from 0.19 through 0.22 MPa$\sqrt{\text{m}}$. These values differ within 5% from those obtained by the surface energy and are very small compared to the reported fracture toughness of single-crystalline monolayer graphene.

Key words: 2D materials, fracture, molecular dynamics simulation, mechanical properties.

1. Introduction

Buckled two-dimensional (2D) hexagonal sheets are part of graphene-like materials family. Besides buckled 2D hexagonal materials with mono-elements, the binary systems XY, where $X = \text{C}, \text{Si}, \text{Ge}, \text{Sn}$ from group IV and $Y = \text{O}, \text{S}, \text{Se}, \text{Te}$ from group VI elements, have been also theoretically predicted [1–3]. Figure 1 illustrates their structure. These buckled XY monolayers are indirect band gap semiconductors. Small strain of about $\leq 3\,\%$ could induce their indirect-to-direct band gap transition [2]. Here, we focus particularly on buckled hexagonal silicon mono-sulfide (SiS) and germanium selenide (GeSe) monolayers, as representative ones of the just above-mentioned XY binary systems. A small tensile strain of 1% was found to be enough to make the indirect-to-direct band gap transition of buckled GeSe [2]. An indirect band gap of buckled SiS depends sensitively on the in-layer strain [1]. Buckled SiS and GeSe are promising 2D materials for optoelectronic and thermoelectric applications [2, 4]. Motivated by their potential applications, their mechanical performance should be investigated.

Mechanical properties of buckled 2D hexagonal SiS and GeSe were reported by Jiang and Zhou [5] from molecular dynamics (MD) studies at 1 K. Using the crack-tip displacement field, Le *et al.* [6] have considered recently the fracture of various buckled 2D hexagonal materials, including SiS and GeSe, by an atomic-scale finite element method, which neglected the temperature effect, hence their work pertained to 0 K.

To the best of the author's knowledge, mechanical properties of these two materials at room temperature remain almost unclear due to their recent prediction. The present work investigates through MD simulations the mechanical properties and fracture at room temperature of buckled 2D hexagonal SiS and GeSe monolayers. The mode-I critical stress intensity factor is computed either from the initial crack length with the corresponding fracture stress of the pre-cracked sheets, and from the surface energy. Present results at room temperature are discussed with those at low temperature.

2. Numerical procedure

2.1. Interatomic potentials

According to the Stillinger–Weber potential [7], the potential energy E of an atomic structure reads:

$$E = E_r + E_\theta, \tag{2.1a}$$

$$E_r = \sum_{e=1}^{M} V_2, \qquad E_\theta = \sum_{e=1}^{N} V_3, \tag{2.1b}$$

$$V_2 = A e^{[\rho/r_{ij} - r_{\max ij}]}(B/r_{ij}^4 - 1), \tag{2.1c}$$

$$V_3 = K e^{[\rho_{ij}/(r_{ij} - r_{\max ij}) + \rho_{ik}(r_{ik} - r_{\max ik})]}(\cos\theta_{ijk} - \cos\theta_0)^2, \tag{2.1d}$$

E_r is the total bond stretching energy. E_θ is the total bond angle bending energy. V_2 and V_3 are the energies associated to the individual bond stretching and the bond angle bending, respectively. M and N are the numbers of bonds and bond angles, respectively. Further detail of the Stillinger–Weber potential is available in [5, 7]. Potential parameters are taken from [5] for SiS and GeSe sheets.

2.2. Molecular dynamics simulation

MD simulations were performed using the Large-scale Atomic/Molecular Massively Parallel Simulator (LAMMPS) code [8]. Temperature may have a significant effect on the fracture hence the simulation was run at room temperature to reveal accurate results. The MD simulation procedure is available in detail in our previous work [9]. The tensile strain rate of $2.5 \times 10^8\,\mathrm{s}^{-1}$ was used with the

NPT method. The reason for the choice of this strain rate was well discussed in our previous work [10]. To save the space, we do not mention the detailed simulation setup that was reported in [9, 10]. We note that computation of elastic constants of solids using the MD simulation with NVT and NPT methods was discussed in [11]. Every sample had approximately squared shape with 99840 atoms, giving the size of 686.0×685.5 Å and 764.8×764.3 Å for SiS and GeSe sheets, respectively. The axial tensile stress σ was recorded during the simulation from atomic stresses as described in our previous work [10]. The VMD package was used for visualization [12].

3. Results and discussion

Table 1 summaries the optimized structure parameters of the studied materials at zero strain at 0 K. The bond length and buckling height, revealed in the present study, agree well with those from previous density functional theory (DFT) calculations by [2, 4, 13]. We consider here pre-cracked sheet with a central crack initially perpendicular to the tensile direction as shown in Fig. 1. Uniaxial tensile stress-strain curves of the pristine sheets and their corresponding pre-cracked ones are almost identical up to fracture points as indicated in Fig. 2. Of course, the fracture occurs much earlier in a pre-cracked sheet than in its corresponding pristine one. A sudden drop in the stress–strain curve demonstrates a brittle fracture. The maximal axial stress and strain at a maximal stress correspond to the fracture stress and fracture strain, respectively. The maximal axial stress of the pristine sheet refers to its fracture strength. Young's modulus Y is determined by a linear fit of the stress strain curve with the axial strain $\varepsilon \in [0, 0.02]$. By denoting t as the sheet's thickness, Yt and σt correspond to 2D Young's modulus and 2D stress, respectively. Our results of Young's modulus, maximal stress, and strain at the maximal stress at 300 K are significantly

Table 1. Optimized structure parameters at zero strain at 0 K. r is the bond length; h is the buckling height, d is the lattice constant. r_1 and r_2 are the Van der Waals radius [18] of the first and second elements in SiS and GeSe sheets. Values in *italic font* with a subscript are taken from DFT calculations by: a) KAMAL *et al.* **[2],** b) TOMÁS *et al.* **[13],** c) KAGDADA *et al.* **[4].**

Sheets	r [Å]	h [Å]	d [Å]	r_1 [Å]	r_2 [Å]	t [Å]
SiS	2.320	1.327	3.297	2.1	1.8	5.23
	2.321[a)]		*3.299*[a)]			
	2.37[b)]	*1.368*[b)]	*3.352*[b)]			
GeSe	2.568	1.449	3.672	2.11	1.9	5.46
	2.568[a)]		*3.676*[a)]			
	2.56[c)]	*1.45*[c)]				

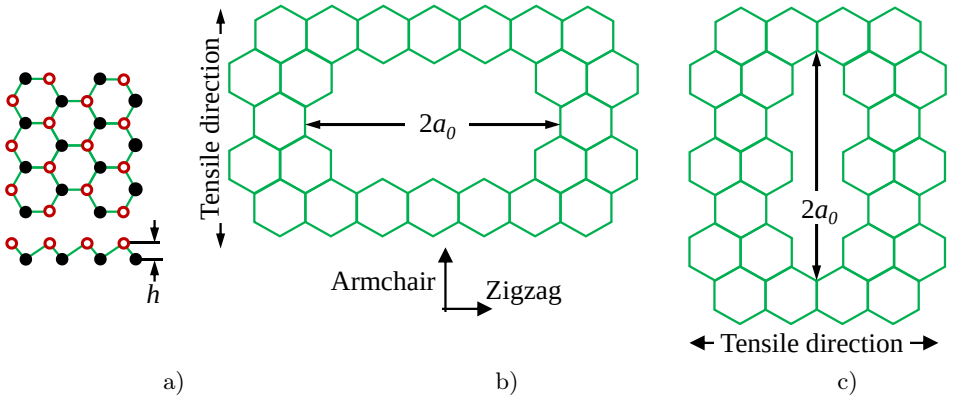

Fig. 1. Schematic illustration of: a) top and side views of a buckled hexagonal sheet; b) top view of a pre-cracked sheet under tension in the armchair direction; c) a pre-cracked sheet under tension in the zigzag direction.

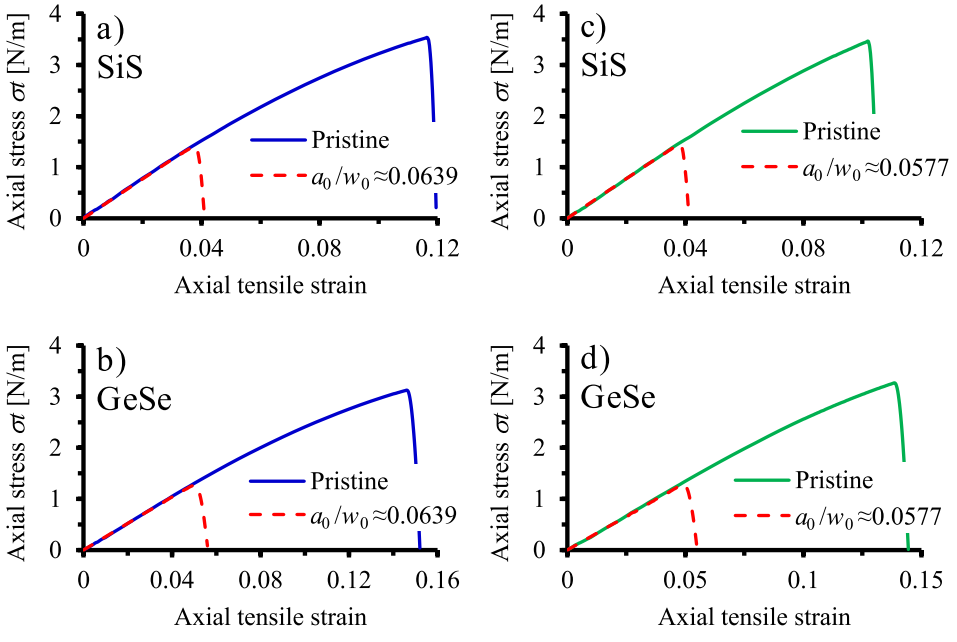

Fig. 2. Uni-axial tensile stress-strain curves of the pristine and pre-cracked sheets (a_0 is the initial half crack length and w_0 is the initial half sheet length along the initial crack direction) under the tension in: a), b) zigzag and c), d) armchair directions.

lower than those from previous MD simulation at 1 K by Jiang and Zhou [5] as shown in Table 2. A reduction of 16–18 % in Young's modulus, 25–32 % in tensile fracture stress due to the temperature is found. The other reason may

Table 2. Tensile mechanical properties at 300 K (ZZ and AC denote the tension along the zigzag and armchair directions, respectively). Values in parentheses are taken from MD study at 1 K with sample size of 100×100 Å by JIANG and ZHOU [5].

Sheets	Young's modulus Yt [N/m]		Maximal stress σt [N/m]		Strain at maximal stress [%]	
	ZZ	AC	ZZ	AC	ZZ	AC
SiS	38.3	38.3	3.54	3.46	11.65	10.2
	(45.8)	(45.5)	(4.9)	(5.1)	(24.0)	(21.0)
GeSe	26.0	26.0	3.13	3.27	14.6	13.85
	(31.5)	(31.6)	(4.2)	(4.4)	(28.0)	(24.0)

be our much larger sample size compared to that of 100×100 Å in the previous work by JIANG and ZHOU [5].

The fracture strength and Young's modulus are almost the same for the tension along the zigzag and armchair directions. 2D Young's modulus of SiS is 38.3 N/m, which is slightly higher than that of buckled monolayer germanene (36–37.5 N/m) estimated by the MD simulation with Tersoff potential at 300 K [9]. 2D Young's modulus of GeSe is 26.0 N/m, which is approximately a half of that of low-buckled monolayer blue phosphorene (50–50.5 N/m) reported from the MD study with the Reax force field at room temperature [10]. 2D fracture strength of SiS and GeSe are ∼3.5 and 3.1–3.3 N/m, respectively. These values of the fracture strength are lower than those of buckled monolayer germanene (4.6–5.1 N/m by MD study with Tersoff potential [9], 4 N/m by MD simulation with the Stillinger Weber potential [14], 4.1–4.7 N/m by DFT calculations [15]), and blue phosphorene (6.4–6.7 N/m) [10].

Figure 3 pertains to the evolution of the fracture strain versus the initial half crack length, showing that the pre-cracked sheet's fracture strain falls below 5.3 % with the initial crack length in the range $a_0/w_0 \in [0.048, 0.1]$, where a_0 is the initial half crack length and w_0 is the initial half sheet length along the

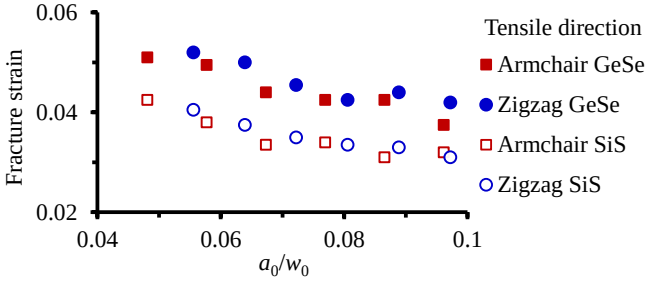

FIG. 3. Evolution of the fracture strain versus the normalized initial half crack length a_0/w_0 under uniaxial tension.

initial crack direction. Figure 2 shows that SiS and GeSe sheets exhibit approximately linearity up to an axial tensile strain of ∼5%, allowing the use of linear fracture mechanics [16] to compute the critical stress intensity factor (or fracture toughness) from the fracture stress σ_f and initial crack length as below:

$$K_{Ic} = \sigma_f \sqrt{\pi a_0}. \tag{3.1}$$

Table 3. Mode-I critical stress intensity factor K_{Ic} and surface energy at 300 K. ZZ and AC denote the tension in the zigzag (initial crack in the armchair direction) and armchair (initial crack in the zigzag one) directions, respectively. Values in parentheses are taken from the atomic-scale finite element simulation with the crack-tip displacement field at 0 K [6].

Sheets	$K_{Ic}t$ [10^{-4} N/m$^{1/2}$]		K_{Ic} [MPa · m$^{1/2}$]		γt [10^{-9} J/m]		$t\sqrt{2\gamma Y}$ [10^{-4} N/m$^{1/2}$]	
	ZZ	AC	ZZ	AC	ZZ	AC	ZZ	AC
SiS	1.168	1.147	0.223	0.219	0.1820	0.1576	1.181	1.099
	(2.03)	(1.85)						
GeSe	1.095	1.058	0.201	0.194	0.2340	0.2026	1.103	1.026
	(1.82)	(1.67)						

The mode-I critical stress intensity factor K_{Ic} remains almost a constant, independent of the initial crack length as clearly indicated in Fig. 4. Their averaged values from tests with different initial crack lengths are listed in Table 3.

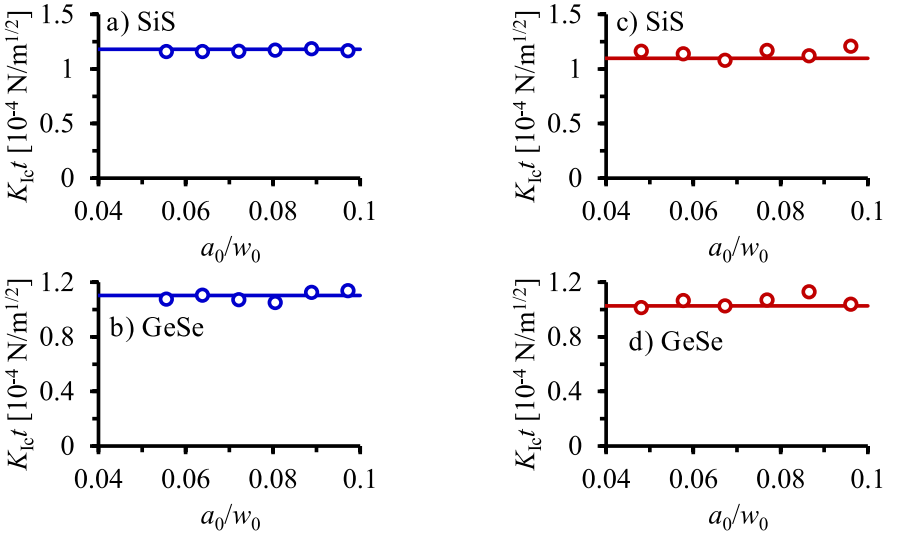

Fig. 4. Stress intensity factor estimated by $K_{Ic} = \sigma_f \sqrt{\pi a_0}$ (displayed by small *circles*) versus the normalized initial half crack length a_0/w_0 under the tension in: a), b) zigzag and c), d) armchair directions. *Solid lines* correspond to $\sqrt{2\gamma Y}$.

The sheet's thickness t is specified as [17]: $t = h + r_1 + r_2$; where h is the buckling height (see Fig. 1); r_1 and r_2 are the Van der Waals radius of the first and second elements in a binary sheet, respectively. The Van der Waals radii are taken from [18] for Si, S, Ge and Se elements, and tabulated in Table 1.

On the other hand, the mode-I critical stress intensity factor K_{Ic} can be evaluated from the surface energy γ as below [16]:

$$K_{Ic} = \sqrt{2Y\gamma}. \tag{3.2}$$

The surface energy γ is evaluated at 300 K from the bond energy at equilibrium at zero strain. This bond energy is calculated by dividing the sheet's potential energy at equilibrium at zero strain by the number of bonds of the sheet. K_{Ic} estimated by the fracture stress with initial crack length from Eq. (3.1) and its corresponding value (also shown in Fig. 4 and Table 3) by the surface energy from Eq. (3.2) differ from each other less than 5 %, indicating that lattice trapping is insignificant for SiS and GeSe sheets. K_{Ic} of SiS and GeSe is estimated at $\sim$0.22 and 0.19–0.2 MPa$\sqrt{\text{m}}$, respectively. These values are very small compared to the values of $\sim 3\,\text{MPa}\sqrt{\text{m}}$ of single-crystalline monolayer graphene at 300 K, see e.g. [19]. Compared to the critical stress intensity factor at 0 K (estimated by the atomic-scale finite element simulation of the crack-tip displacement field [6]) listed in Table 3, the corresponding values at 300 K in the present study are about 36–42 % lower. When increasing temperature from 0 K to 300 K, Young's modulus and tensile fracture stress of the pristine sheets reduce about 16–18% and 25–32%, respectively, as shown in Table 2. Pre-broken bonds in a pre-cracked sheet weaken certainly the bonds at a crack tip. Atomic fluctuation due to the temperature is possibly larger around the crack tip in a pre-cracked sheet than in its corresponding pristine one. Hence, temperature affects much on the fracture but less on Young's modulus. This issue should be further studied in the future.

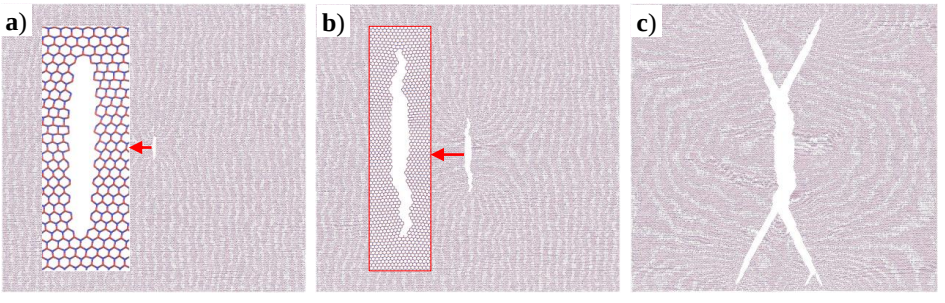

FIG. 5. Snapshots of the buckled GeSe sheet under uniaxial tension in the zigzag direction (*horizontal direction*) with a centered pre-crack of initial length $2a_0 = 32r_p$ ($a_0/w_0 \approx 0.089$, $r_p = \sqrt{r^2 - h^2}$) at a: a) axial tensile strain $\varepsilon = 4.0\,\%$; b) $\varepsilon = 4.5\,\%$; c) $\varepsilon = 5.0\,\%$. The tensile strain at maximal stress is $\sim$4.4%. Red narrow indicates a magnification of the crack region.

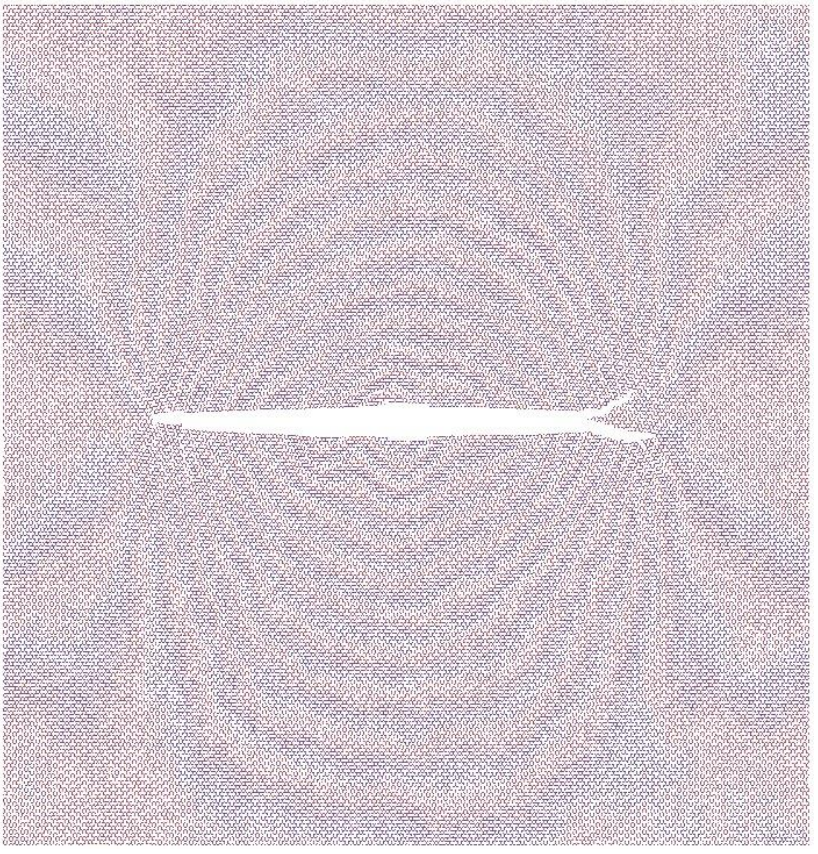

Fig. 6. Snapshots of the buckled SiS sheet under uniaxial tension in the armchair direction (*vertical direction*) with a centered pre-crack of initial length $2a_0 = 12d$ ($a_0/w_0 \approx 0.058$) at an axial tensile strain $\varepsilon = 4.0\,\%$ (d is the lattice constant). The tensile strain at maximal stress is ∼3.8%.

SiS and GeSe exhibit similar fracture mechanisms with crack kinking, branching, and meandering for both the tension along the zigzag (initial crack in the armchair direction) and armchair (initial crack in the zigzag direction) directions as shown in Figs. 5 and 6.

4. Conclusions

In summary, the mechanical and fracture properties of buckled 2D hexagonal monolayer SiS and GeSe sheets were studied by MD simulation at 300 K. Fracture strength and Young's modulus are almost the same for the tension along the zigzag and armchair directions. 2D Young's modulus of SiS and GeSe are 38.3 and 26.0 N/m, respectively. 2D fracture strength is ∼3.5 N/m for SiS, and

3.1–3.3 N/m for GeSe. Young's modulus and fracture strength of SiS and GeSe are lower than those of buckled monolayer blue phosphorene. Mode-I critical stress intensity factor was computed either from the initial crack length with the corresponding fracture stress, and from the surface energy. Deviations of the fracture toughness estimated by these 2 methods are less than 5 %. Mode-I fracture toughness of SiS and GeSe appears in the range from 0.19 to 0.22 MPa$\sqrt{\text{m}}$. These values are very small compared to the reported fracture toughness of single-crystalline monolayer graphene.

Conflict of interest

The Author declares no conflict of interest.

Acknowledgements

This work was supported by Vietnam National Foundation for Science and Technology Development (NAFOSTED) under the grant no. 107.02-2020.09.

References

1. Z. ZHU, J. GUAN, D. LIU, D. TOMÁNEK, *Designing isoelectronic counterparts to layered group V semiconductors*, ACS Nano, **9**, 8, 8284–8290, 2015.
2. C. KAMAL, A. CHAKRABARTI, M. EZAWA, *Direct band gaps in group IV-VI monolayer materials: binary counterparts of phosphorene*, Physical Review B, **93**, 12, 125428, 2016.
3. H. ARKIN E. AKTÜRK, *Investigation of adatom adsorption on single layer buckled germanium selenide*, Applied Surface Science, **390**, 185–189, 2016.
4. H.L. KAGDADA, P.K. JHA, P. ŚPIEWAK, K.J. KURZYDŁOWSKI, *Understanding the behavior of electronic and phonon transports in germanium based two dimensional chalcogenides*, Journal of Applied Physics, **124**, 23, 235701, 2018.
5. J.-W. JIANG, Y.-P. ZHOU, *Handbook of Stillinger-Weber Potential Parameters for Two-Dimensional Atomic Crystals*, INtechOpen, 2017.
6. M.-Q. LE, H.-T. NGUYEN, T.-L. BUI, *Fracture of 28 buckled two-dimensional hexagonal sheets*, Mechanics of Advanced Materials and Structures, 1–13, 2021.
7. F.H. STILLINGER T.A. WEBER, *Computer simulation of local order in condensed phases of silicon*, Physical Review B, **31**, 8, 5262, 1985.
8. S. PLIMPTON, *Fast Parallel Algorithms for Short-Range Molecular Dynamics*, Journal of Computational Physics, **117**, 1, 1–19, 1995.
9. M.-Q. LE, *Fracture of monolayer germanene: a molecular dynamics study*, International Journal of Modern Physics B, **32**, 22, 1850241, 2018.
10. M.-Q. LE, *Reactive molecular dynamics simulations of the mechanical properties of various phosphorene allotropes*, Nanotechnology, **29**, 19, 195701, 2018.

11. G. Clavier, N. Desbiens, E. Bourasseau, V. Lachet, N. Brusselle-Dupend, B. Rousseau, *Computation of elastic constants of solids using molecular simulation: comparison of constant volume and constant pressure ensemble methods*, Molecular Simulation, **43**, 17, 1413–1422, 2017.

12. W. Humphrey, A. Dalke, K. Schulten, *VMD: visual molecular dynamics*, Journal of Molecular Graphics, **14**, 1, 33–38, 1996.

13. T. Alonso-Lanza, A. Ayuela, F. Aguilera-Granja, *An array of layers in silicon sulfides: Chainlike and monolayer*, Physical Review B, **94**, 24, 245441, 2016.

14. M.H. Rahman, E.H. Chowdhury, D.A. Redwan, S. Hong, *Computational characterization of thermal and mechanical properties of single and bilayer germanene nanoribbon*, Computational Materials Science, **190**, 110272, 2021.

15. B. Mortazavi, O. Rahaman, M. Makaremi, A. Dianat, G. Cuniberti, T. Rabczuk, *First-principles investigation of mechanical properties of silicene, germanene and stanene*, Physica E: Low-dimensional Systems and Nanostructures, **87**, 228–232, 2017.

16. T.L. Anderson, *Fracture Mechanics – Fundamentals and Applications*, 4th ed., CRC Press, USA, 2017.

17. P. Hess, *Thickness of elemental and binary single atomic monolayers*, Nanoscale Horizons, **5**, 3, 385–399, 2020.

18. M. Mantina, A.C. Chamberlin, R. Valero, C.J. Cramer, D.G. Truhlar, *Consistent van der Waals radii for the whole main group*, The Journal of Physical Chemistry A, **113**, 19, 5806–5812, 2009.

19. B. Zhang, L. Mei, H. Xiao, *Nanofracture in graphene under complex mechanical stresses*, Applied Physics Letters, **101**, 12, 121915, 2012.

Received September 03, 2021; revised version January 11, 2022.
Published online February 01, 2022.